Available online at www.sciencedirect.com

ScienceDirect

Solar Energy 103 (2014) 200–209

SOLAR ENERGY

www.elsevier.com/locate/solener

Smart windows: Thermal modelling and evaluation

M. Sabry [a,b,*], P.C. Eames [c], H. Singh [d], Yupeng Wu [e]

[a] Physics Dept., College of Applied Science, Umm Al Qura University, Makkah,Saudi Arabia
[b] National Research Institute of Astronomy and Geophysics, Cairo, Egypt
[c] CREST, Loughborough University, Loughborough LE11 3TU, UK
[d] School of Engineering and Design, Brunel University, Uxbridge UB8 3PH, UK
[e] School of Engineering, Nottingham University, UK

Received 20 July 2013; received in revised form 31 January 2014; accepted 6 February 2014

Communicated by: Associate Editor G.N. Tiwari

Abstract

A numerical investigation of the performance of a multi paned smart window integrated with water-cooled high efficiency third generation GaAsP/InGaAs QWSC (~32% efficiency) solar cells illuminated by two-axis tracking solar concentrators at 500× in the inter pane space is presented. Optimising system parameters such as optical concentration ratio and coolant (water) flow rate is essential in order to avoid degradation in system performance due to high cell temperatures and thermal stresses. Detailed modelling of the thermo-fluid characteristics of the smart windows system was undertaken using a finite volume CFD package. Results of this analysis which considered the conductive, convective and radiative heat exchange processes taking place in the interior of the smart window system as well as the heat exchange to the internal and external ambient environment are presented.
© 2014 The Authors. Published by Elsevier Ltd. This is an open access article under the CC BY license (http://creativecommons.org/licenses/by/3.0/).

Keywords: Smart windows; Photovoltaic; Facades; CFD

1. Introduction

Solar energy is increasingly being recognised as one of the main substitutes for fossil fuels due to its essentially non-polluting inexhaustible nature. Photovoltaic/thermal (PV/T) solar collectors, first proposed by (Kern and Russell, 1978), yield a higher utilisable energy output per unit collector area (Tripanagnostopoulos et al., 2007; Vats and Tiwari, 2012). The approach of combining a thermal and PV component is considered more appropriate for concentrating solar systems in which heat removal from the PV cells will be a critical issue.

Currently different types of double-skin façades are employed in buildings to provide increased thermal comfort while lowering space heating and cooling energy consumption (Safer et al., 2005a). Solar radiation is comprised of both long and short wave radiation, i.e., heat and light. When seeking to regulate the amount of solar radiation entering into a building, the challenge is to achieve desired levels of daylight intensity without excess introduction of the concomitant heat. Excessive direct solar insolation in the interior space, workplace or home, can lead to discomfort due to high levels of glare when the sun is directly in the field of view or is specularly reflected from indoor surfaces (Kim et al., 2009; Piccolo and Simone, 2009) and should be avoided. Blinds are frequently used within such façades to control the intensity of the incident direct solar radiation component by

* Corresponding author at: Physics Dept., College of Applied Science, Umm Al Qura University, Makkah, Saudi Arabia. Tel.: +966 (0) 566627680.
E-mail address: Mohamed.ma.sabry@gmail.com (M. Sabry).

http://dx.doi.org/10.1016/j.solener.2014.02.016
0038-092X/© 2014 The Authors. Published by Elsevier Ltd.
This is an open access article under the CC BY license (http://creativecommons.org/licenses/by/3.0/).

Nomenclature

D_h	depth of horizontal window segment (m)
D_v	depth of vertical window segment (m)
D_{vc}	depth of the differentially heated vertical cavity (m)
d_e	external tube diameter (m)
d_i	internal tube diameter (m)
H_h	height of horizontal window segment (m)
H_v	height of vertical window segment (m)
H_{vc}	height of the differentially heated vertical cavity (m)
h_{cback}	heat transfer coefficient of back window pane ($Wm^{-2} K^{-1}$)
h_{ccell}	heat transfer coefficient of solar cell ($Wm^{-2} K^{-1}$)
h_{cfront}	heat transfer coefficient of front window pane ($Wm^{-2} K^{-1}$)
h_{clens}	heat transfer coefficient of Fresnel lens ($Wm^{-2} K^{-1}$)
h_{ctube}	tube-air heat transfer coefficient ($Wm^{-2} K^{-1}$)
h_{cwater}	water-tube heat transfer coefficient ($Wm^{-2} K^{-1}$)
W_h	width of horizontal window segment (m)
W_v	width of vertical window segment (m)
X	optical concentration ratio

Greek symbols

η_{cell}	solar cell electrical efficiency
μ_τ	turbulent viscosity (Pa s)
ρ_{cell}	solar cell reflectivity
ρ_g	reflectivity of window pane
ρ_{lens}	reflectivity of Fresnel lens
ρ_{tube}	reflectivity of copper tube
τ_{cell}	solar cell transmissivity
τ_g	transmissivity of window pane
τ_{lens}	transmissivity of Fresnel lens
τ_{tube}	transmissivity of copper tube

blocking the radiation from entering the building and thus reducing the cooling loads. However, these do not use the intercepted solar energy. A smart window, illustrated in Fig. 1, aims to control and regulate solar energy influx through such double skin façades to the interior of buildings. Glass coated with thin films that can change their optical properties reversibly from transparent to opaque when heated and cooled (Bange, 1999), or when subject to an applied electrical current are of great interest (DeForest et al., 2013), again however they do not utilise the incident solar energy for electricity production.

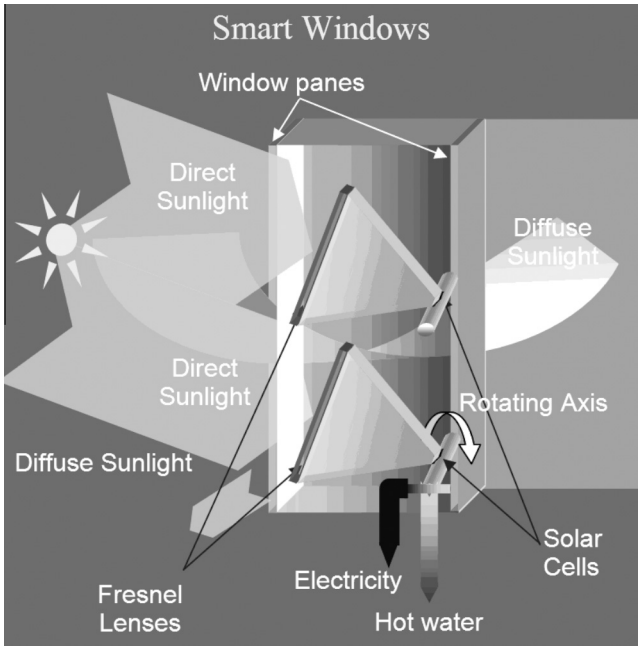

Fig. 1. A conceptual arrangement of a smart window showing its operation.

We examine a new concept of smart windows whereby water cooled concentrator-PV cell units are incorporated inside the gap between two panes of a double glazed window. Two-axis tracking Fresnel lens concentrators coupled to actively cooled high efficiency PV cells have been simulated.

Optical concentration ratio is defined as the ratio between the aperture area to the collector area, while the effective concentration ratio is calculated taking into account the reflection from both aperture and collector surfaces. PV cells considered in this study are the Quantum Well (QW) square solar cells, having area of 16 mm^2 which were reported to achieve efficiency of ~32% under an effective concentration ratio of 500× (Adams et al., 2011; Rohr et al., 2006). The variation of the cell efficiency with concentration ratio is shown in Fig. 2.

When incorporated into a double skin building façade, a point focus or linear Fresnel lens will separate the direct (beam) solar radiation from the diffuse component and concentrate the former on the solar cell whilst facilitating the passage of diffuse radiation into the interior of buildings. Such multifunctional smart windows are able to (i) generate electricity, (ii) block direct sunlight with consequent reduction in building energy cooling load, (iii) transmit diffuse sunlight to provide natural daylight and (iv) provide domestic hot water.

The following system parameters need to be optimised to achieve maximum thermal, optical and electrical performance:

- The optical concentration ratio that provides the best solar to electrical conversion efficiency of the solar cell, taking into account the reduction in performance that results from increased operating temperature.

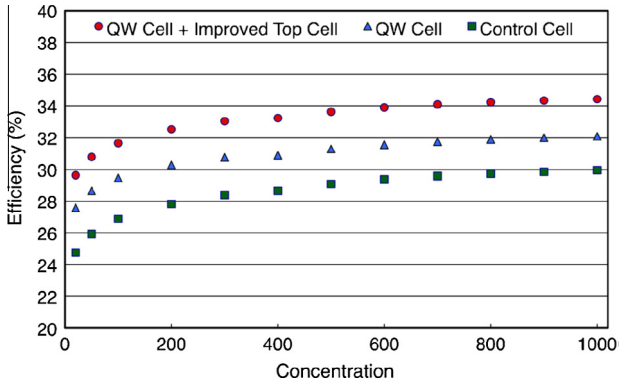

Fig. 2. Electrical conversion efficiency variation of the QW solar cell with optical concentration ratio.

- Heat removal and water flow rate that provides water at a usable temperature while avoiding performance degradation and cell damage that could result from overheating.
- Distribution and spacing of the concentrator systems with each unit comprising a lens and solar cell located at its focus, and the gap between the window panes to maximise the electrical output while maintaining required levels of daylight in the building interiors.

2. Adopted numerical modelling approach

Detailed analysis of the conductive, convective and radiative heat transfer processes occurring within the double glazing that forms the envelope of the smart window has been undertaken employing a finite volume algorithm using STAR CCM, a commercially available CFD package. A double glazing measuring 1 m × 1 m was chosen to closely imitate a commonly available commercial window size. A taller window might result in building up cavity air temperature whereby the upper cell arrays will operate at higher temperatures with lower electrical conversion efficiency compared to the lower arrays as discussed in Section 3.2. Similarly, a wider window might result in heating up of the solar cells near the cooling water exit reducing their electrical conversion efficiency. Window panes were assumed to be 6 mm thick to protect the smart windows interior which contained solar cells measuring 4 mm × 4 mm and Fresnel lenses of dimensions 100 mm × 100 mm.

For accurate simulation of both air and water fluid flow inside the window a relatively small finite volume base size was required resulting in a very number of meshing volumes. This prevented the full window system from being modelled concurrently with the available computing resource. Modelling was thus limited to certain sections of the smart window system. In order to gain improved understanding of internal heat transfer in a smart window the following temperature fields have been studied:

(i) Horizontal temperature profile from water inlet to exit cross-sections in a horizontal window section (H_h, W_h and D_h of 0.2 m, 1 m and 0.1 m respectively) containing five equally spaced concentrator units (each with a Fresnel lens and a PV cell) and the front and back window panes as shown in Fig. 3(a)

(ii) Vertical temperature build-up and accumulation of the top of the window cavity due to natural convective motion of air in a vertical window section (H_v, W_v and D_v of 1 m, 0.2 m and 0.1 m respectively) containing five equally spaced copper tubes fitted in parallel, one with each concentrator unit in addition to the front and back window panes as shown in Fig. 3(b)

The specified arrangement was such that there were five PV cells equidistantly located on each horizontal copper tube through which cooling water flowed. This horizontal segment allowed investigation of the increase in temperature of water flowing inside the tube and a prediction of the final water outlet temperature and operating temperatures of the five solar cells attached to the copper tube enabling the water flow rate required to maintain the temperature of the farthest downstream PV cell to be maintained at an acceptable value to be determined. The

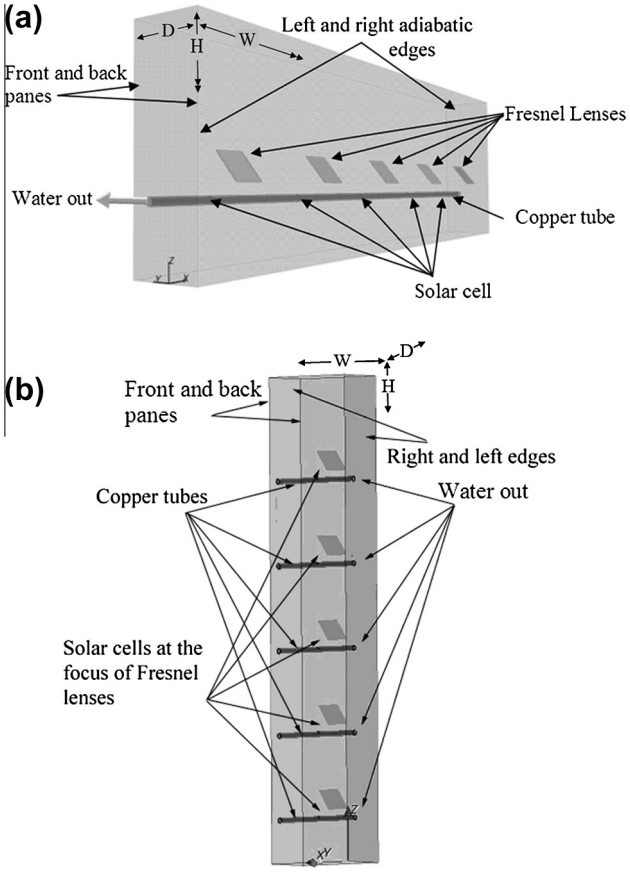

Fig. 3. Modeled window sections (a) horizontal and (b) vertical showing the different components.

vertical section enabled the likely thermal stratification inside a real window to be evaluated and temperatures at the various components in the window predicted.

All radiation incident on the cell, which has not been converted into electricity (due to efficiency limitation) have been assumed to have been converted into heat and accounted for in the thermal radiative exchange calculations in the analysis.

The average temperature of water flowing inside the tube in the horizontal window section was calculated at six cross sectional planes normal to the tube's long axis located at 0.0 m (inlet), 0.2 m, 0.4 m, 0.6 m, 0.8 m and at 1.0 m (outlet). The water temperature was calculated based on the area-weighted average of the water temperature distribution profile in each of the planes. Solar cells were located at 0.1 m, 0.3 m 0.5 m, 0.7 m and 0.9 m along the copper tube, the temperatures reported are the average of the solar cell surface temperatures. In all of the following graphs showing water and solar cell temperatures, the measurement locations are referred to as the distance along the horizontal x-axis rather than the cross sectional plane or solar cell numbers. Water flow through copper tubes is assumed to be steady, incompressible and laminar.

Pumping power has not been introduced in the modelling since the focus of the study presented in this paper is onto the thermal modelling of the smart window and reducing solar cells temperatures for optimal efficiency.

The sections under test were meshed using tetrahedral cell shaped mesh elements. Fig. 4 shows a cross section of one concentrator unit normal to the window panes illustrating the generated mesh and the different components. The construction of the volume mesh influences the rate of convergence and the accuracy of the final solution. Volume mesh are constructed to give adequate resolution in regions where spatial gradients are high, namely, solar cells, air and copper tube regions around them as shown in Fig. 4. In order to make sure that simulation results are independent of the mesh, a grid sensitivity study with different base-size and growth-rate meshes has been performed applying same boundary conditions listed, establishing the same solution features.

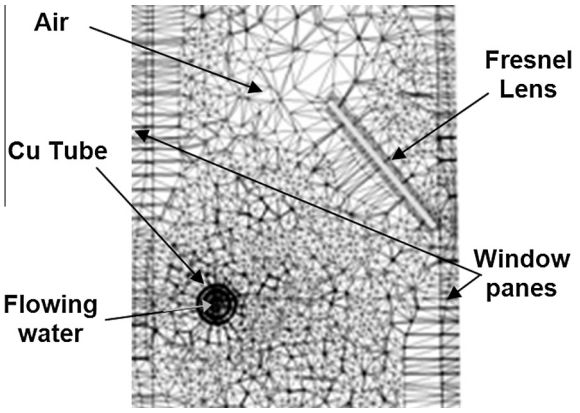

Fig. 4. Cross section of meshed unit showing the different finite volumes.

2.1. Simulation of a differentially heated rectangular vertical cavity

To establish the validity of the model of the smart window developed, it was first employed to simulate a differentially heated air-filled rectangular vertical cavity typical of a full-sized (1 m × 1 m) double glazed window (Fig. 5) and the results were verified against those previously published by Safer et al. (2005b), as shown in Fig. 6. Boundary conditions assumed are such that the front window pane is assumed to receive a uniform radiative flux with all four side walls being adiabatic. Simulation of one horizontal window segment, complete with PV cells, lenses, and heat removal tubes was then undertaken with the boundary conditions detailed in Table 1. Natural convective heat transfer in a differentially heated air-filled vertical cavity formed by

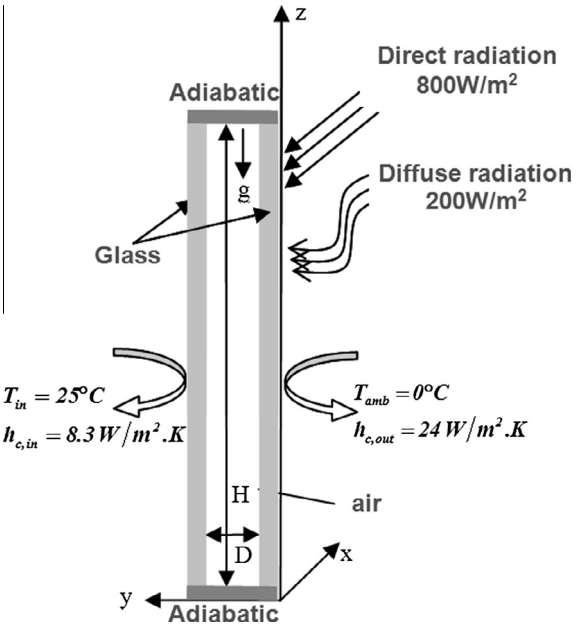

Fig. 5. A schematic of the simulated window and the assumed thermal boundary conditions.

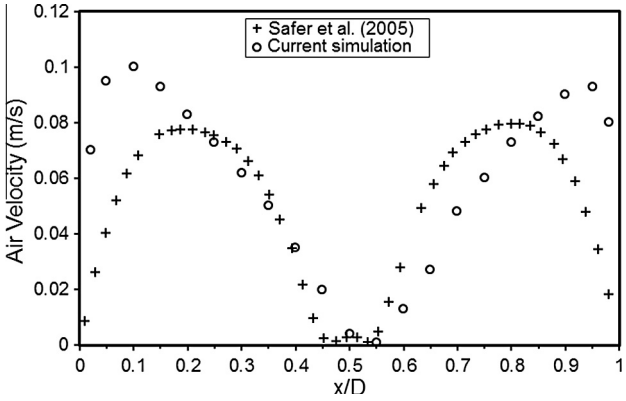

Fig. 6. Comparison between simulation by Safer et al. and current simulation of air velocity inside the differentially heated vertical cavity.

Table 1
Boundary conditions and material properties.

Boundary conditions and material	Physical value/boundary property
Window panes	
Material	Glass
Reflectivity R_g	8%
Transmissivity T_g	91%
Wall specification	Smooth, no-slip
Front pane	
Heat transfer coefficient h_{cf}	24 W/m^2 K
Thermal specification	Uniform heat flux, convection, Surface to surface heat transfer
Back pane	
Heat transfer coefficient h_{cb}	8.3 W/m^2 K
Thermal specification	Convection, surface to surface heat transfer
Window sides	Adiabatic
Fresnel lenses	
Heat transfer coefficient h_{ct}	In-field calculated
Material	Acrylic
Reflectivity R_l	12%
Thermal specification	Convection, surface to surface heat transfer
Transmissivity T_l	85%
Wall specification	Smooth, no-slip
Tube	
Heat transfer coefficient h_{ct}	In-field calculated
Material	Copper
Reflectivity R_t	8%
Thermal specification	Convection, surface to surface heat transfer
Transmissivity T_t	0
Wall specification	Smooth, no-slip
Water	
Heat transfer coefficient h_{cw}	50 W/m^2 K
Thermal specification	Convection
Solar cells	
Electrical efficiency	~32%
Heat transfer coefficient h_{ct}	In-field calculated
Material	GaAsP/InGaAs QWSC
Reflectivity R_{sc}	5%
Thermal specification	Convection, conduction, surface to surface heat transfer
Transmissivity T_t	0

two glass panes with an aspect ratio (H_{vc}/D_{vc}) of 10, Fig. 5, has been simulated assuming an intensity of 800 W/m^2 of direct and 200 W/m^2 of diffuse solar radiation incident on the outer window pane with an ambient external temperature of 0 °C, and a building interior temperature of 25 °C. In these simulations the realizable two-layer – turbulence model (Shih et al., 1994) was used. In this model, C_μ, a critical coefficient of the model is expressed as a function of mean flow and turbulence properties, rather than assumed to be constant as in the standard model. This allows the model to satisfy certain mathematical constraints on the normal stresses consistent with the physics of turbulence (realizability). The concept of a variable is also consistent with experimental observations in boundary layers. The realizable – model is substantially better than the standard – model and is implemented in STAR-CCM with a two-layer approach, which enables it to be used with fine meshes that resolve the viscous sub-layer. The turbulent viscosity, μ_t, is expressed as:

$$\mu_t = \frac{\rho C_\mu k^2}{\varepsilon} \tag{1}$$

where C_μ is a coefficient given by $C_\mu = \frac{1}{A_0 + A_s U^{(*)} \frac{k}{\varepsilon}}$ (2)

ρ is the density, $U^{(*)}$ is a function of strain rate tensor and vorticity tensor, A_0 is whose value is taken as 4.0.

A_s is whose value is taken as $A_s = (\sqrt{6})\cos\phi$ (3)

Contours obtained indicating internal air velocity (magnitude and direction) and temperatures at planes parallel and normal to the glass panes are shown in Fig. 7 with Fig. 7(a) showing the velocity magnitude and direction (−ve and +ve relative to the vertical axis of the cavity) in the mid plane normal to the glass panes, Fig. 7(b) temperature distribution at the plane in the middle of the cavity parallel to the windows panes and Fig. 7(c) temperature distribution at a plane half way up the cavity normal to the panes.

The outer and inner window panes were predicted to be about 7 °C and 20 °C respectively, with a difference in temperature of about 6 to 8 °C between the bottom and top in the mid-plane of the air enclosed in the double glazing.

2.2. The water-cooled solar cell system

Solar cell performance is sensitive to its operating temperature. Active cooling using water as the coolant was used to maintain a desired solar cell operating temperature additionally delivering hot water to displace water heating needs. The subsystem of a solar cell attached to the exterior of a 0.2 m long copper tube ($d_i = 8$ mm, $d_e = 12$ mm) with cooling water flowing inside was separately simulated and optimised. The solar cell was assumed to be operating under a concentration ratio of 500×, with a direct solar radiation intensity of 800 W/m^2 prior to concentration. Both cell temperature and the difference between average water inlet and outlet temperatures were predicted for a range of water flow rates (0.0025–0.03 kg/s) assuming fixed convective heat transfer coefficients of 50 W/m^2 K inside the tubes and an initial estimate of 1 W/m^2 K for the outside tube surface. As can be seen in Fig. 8 doubling the flow rate from 0.01 to 0.02 kg/s decreased the predicted solar cell temperature and the water outlet temperature respectively by approximately 0.4 °C and 1.5 °C. To achieve the best trade-off between high water outlet temperature, low solar cell temperature and low pumping power required, water flow rates of 0.01 kg/s and 0.02 kg/s with a convective heat transfer coefficient inside the tubes of 50 W/m^2 K were adopted for full system simulations.

Fig. 9(a) illustrates the temperature distribution at a cross section through the copper tube from the water inlet

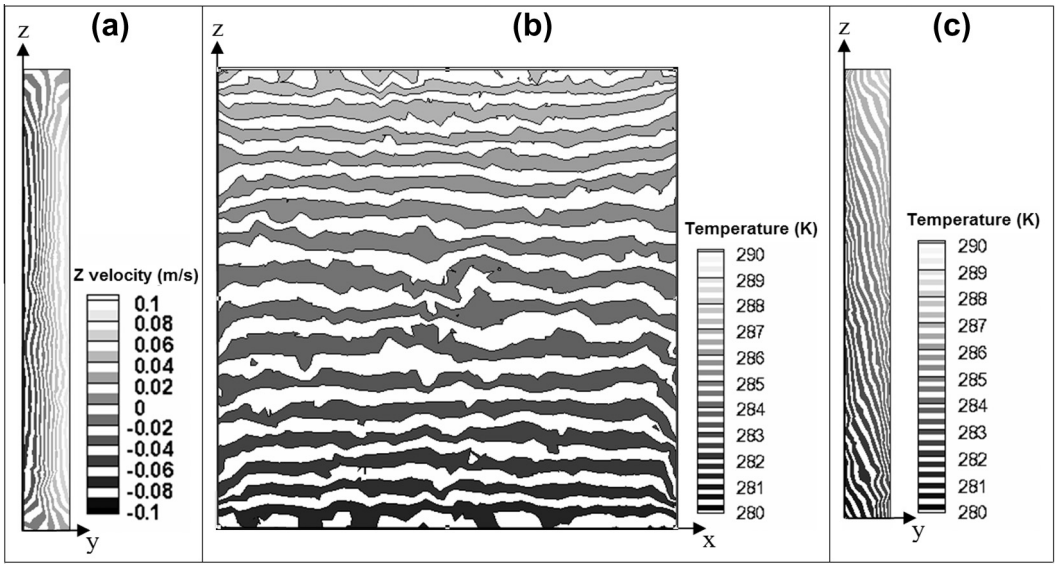

Fig. 7. Contours of (a) internal air velocity z component (m/s), and (b) temperature (K) parallel and (c) normal to the glass panes at mid planes.

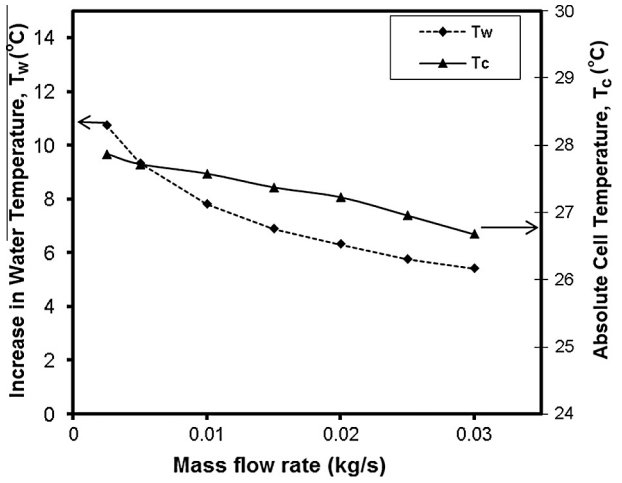

Fig. 8. Predicted absolute cell temperature and increase in water temperature for different water flow rates.

to the outlet with the illuminated solar cell located half way along the tube. With the inlet temperature fixed at 10 °C, the absolute cell temperature is about 27.6 °C as shown in Fig. 9(b).

3. Thermal performance of the window

3.1. Predicted cavity air temperatures

It is important to predict the expected temperatures at different sections within the cavity air as well as that on the front and back surfaces of the window. A series of simulations were performed whilst dividing the window in five equally sized and distinct vertical sections (H_v, W_v and D_v of 1 m, 0.2 m and 0.1 m respectively) employing the boundary conditions listed in Table 1 and the physical conditions listed in Table 2. To enable a full 1 m × 1 m window to be simulated, the predictions obtained for the boundary of the first section were used as the boundary conditions for the second section with the process repeated for the remaining three sections. Results from the five vertical window segments have been gathered to study the performance of the complete window. Fig. 10(a) shows temperature profiles on a plane normal to the window panes and Fig. 10(b) on a plane parallel to the window panes and passing through the five solar cells located on five horizontal tubes at the third segment as a sample. The temperature profiles presented indicate thermally stratified air in the

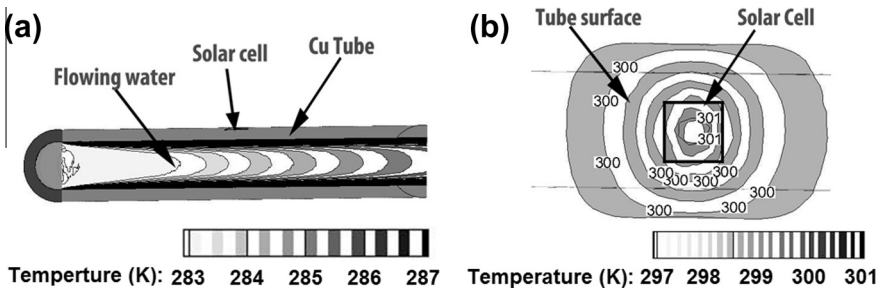

Fig. 9. Temperature distribution (K) of: (a) cross section through the copper tube and (b) solar cell and the surrounding Cu tube surface for a water flow rate of 0.01 kg/s.

Table 2
Physical conditions applied on simulation of vertical window segment.

Property	Value
Water flow rate	0.01 kg/s
Incident direct solar radiation	800 W/m^2
Inside (building) temperature	297 K
Outside (ambient) temperature	273 K
Water inlet temperature	283 K

Table 3
Physical conditions employed for the simulation of the horizontal window section.

Property	Value
Water flow rate	0.02 kg/s
Incident direct solar radiation	800 W/m^2
Inside (building) temperature	293 K
Outside (ambient) temperature	273 K
Water inlet temperature	283 K

window. Fig. 10(c) shows the velocity (m/s) of air inside the window caused by natural convection with close-up air flow around the heated solar cell. It is shown that there existed a temperature differential of nearly 20 °C between the top and bottom air layers.

Designers must design smart windows to facilitate higher natural convective motion of the cavity air allowing the top half of the window to operate at a lower temperature to achieve a higher electrical conversion efficiency.

3.2. Predicted solar cell and water temperatures

Thermal performance of the smart window has been predicted under different simulated parameters namely, direct solar radiation intensity, ambient temperature, water inlet temperature, and water flow rate. Fig. 11 shows a sample of temperature distribution of all window components at a plane passing through the horizontal window segment based on simulation physical conditions listed on Table 3. Simulation data has been collected from all successive simulations. The effect of increasing direct solar radiation on both solar cells and water temperatures is shown in Fig. 12. Three different simulations were performed assuming direct solar radiation intensities of 400, 600, and 800 W/m^2 incident on the window's front pane with set ambient temperature, water inlet temperature and water flow rate of respectively 273 K, 283 K and 0.01 kg/s. Water temperature was found to increase by 5 °C as it passed through the tube, carrying the solar cells, from left to right for the bottom most units at 800 W/m^2 of direct incident solar radiation.

The effect of increasing the external ambient temperature was also investigated by employing three different ambient temperatures of 273 K, 293 K, and 323 K as boundary conditions at the front window pane external surface for a water inlet temperature of 293 K, a direct

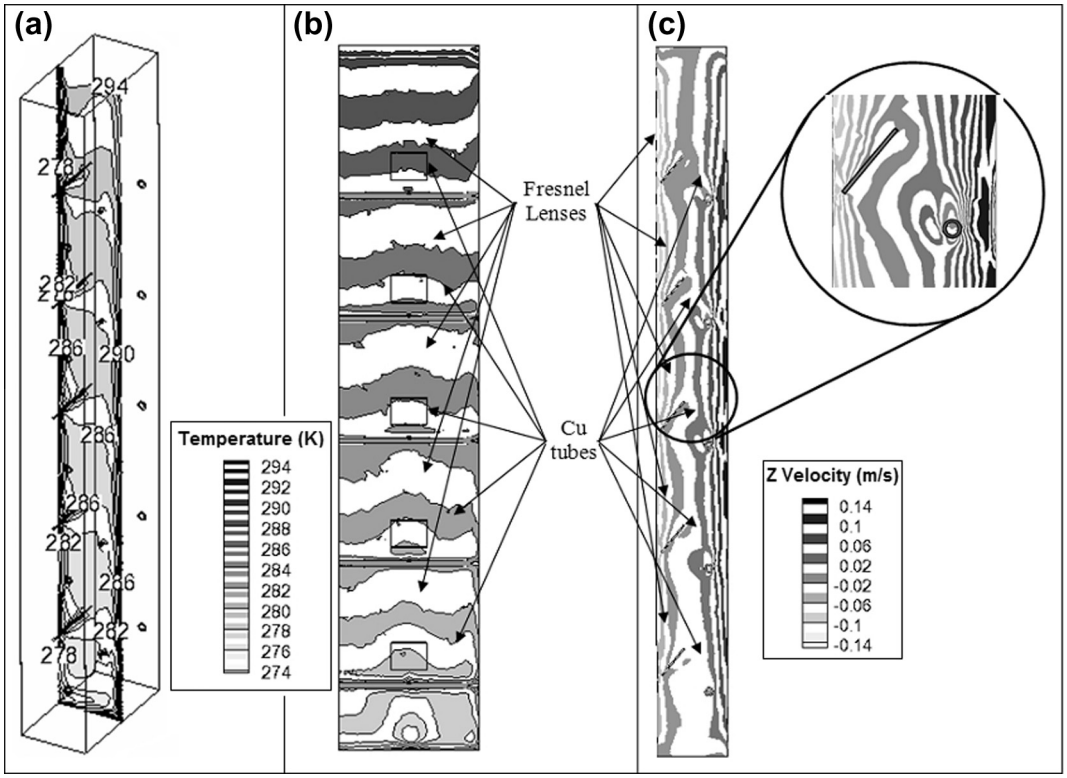

Fig. 10. Vertical window segment across sectional planes (a) plane normal to the window panes, (b) plane parallel to the window panes both passing through tubes and solar cells showing temperature (K) distribution, and (c) plane normal to the window panes and passing through the centre of the segment width showing velocity (m/s) distribution or air inside smart window cavity.

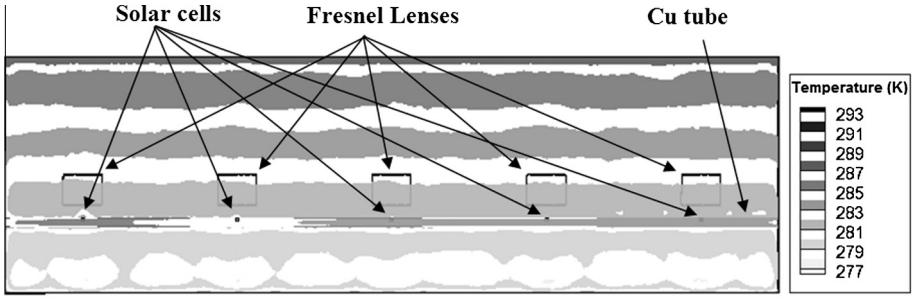

Fig. 11. Temperature (K) distribution inside the horizontal segment at a plane passing through the solar cells and the tube.

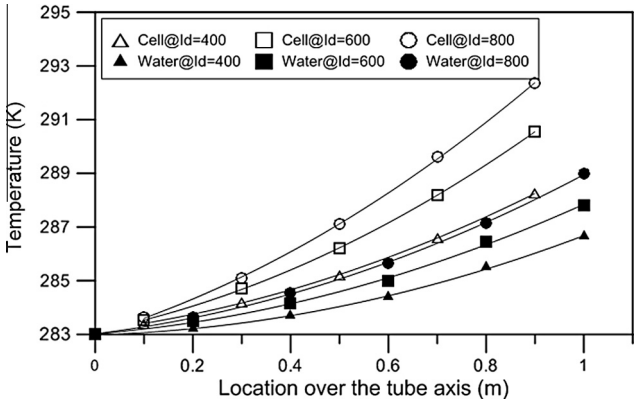

Fig. 12. Solar cell and water temperatures predicted at different locations over the tube axis for three different direct solar radiation intensities of 400, 600, and 800 W/m^2 with constant ambient and water inlet temperatures of 273 K, and 283 K respectively at a water flow rate of 0.01 kg/s.

radiation intensity of 800 W/m^2 and a water flow rate of 0.01 kg/s. Resulting water and cell temperatures are shown in Fig. 13. A 50 °C increase in external ambient temperature, from 273 K to 323 K, resulted in a negligible rise, 0.3 °C and 0.5 °C, in last solar cell and water outlet temperatures located at 0.9 m and 1 m respectively.

Increasing water inlet temperature had a significant effect on the thermal performance of smart window shown in both cell and water temperatures. This effect was simulated for two different ambient temperatures of 293 K and 323 K. Fig. 14 gives cells and water exit temperatures at three different water inlet temperature of 283 K, 293 K, 303 K keeping the ambient temperature, direct solar radiation and flow rate at 293 K, 800 W/m^2, and 0.01 kg/s respectively. Fig. 15 shows the cell and water exit

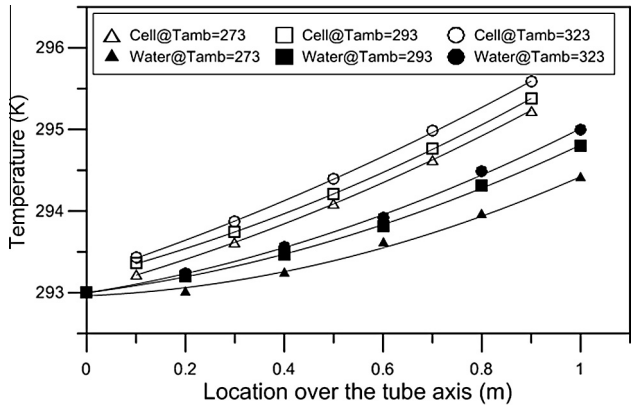

Fig. 13. Cell and water temperatures (K) predicted at different locations over the tube axis for ambient external temperatures of 273 K, 293 K, and 323 K respectively assuming constant water inlet, incident direct radiation and water flow rate are 293 K, 800 W/m^2 and 0.01 kg/s respectively.

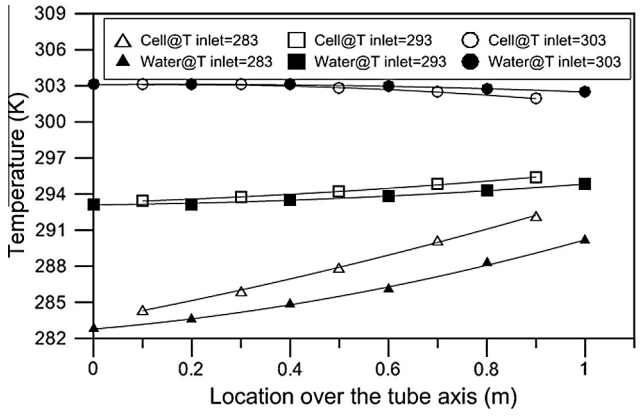

Fig. 14. Cell and water temperatures predicted at different locations over the tube axis for three different water inlet temperature of 283 K, 293 K, and 303 K with constant external ambient temperature, direct solar radiation and flow rate of 293 K, 800 W/m^2, and 0.01 kg/s respectively.

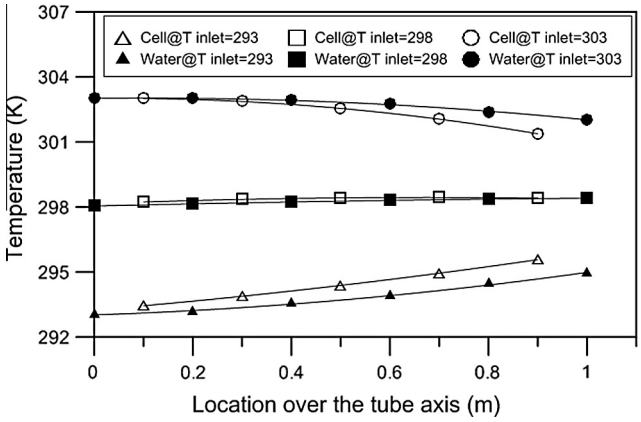

Fig. 15. Cell and water temperatures predicted at different locations over the tube axis for three different water inlet temperatures of 293 K, 298 K, and 303 K with constant external ambient temperature, direct solar radiation and flow rate at 323 K, 800 W/m^2, and 0.01 kg/s respectively.

temperatures predicted for a higher ambient temperature of 323 K and water inlet temperatures of 293 K, 298 K and 303 K with direct solar radiation and flow rate at 800 W/m^2, and 0.01 kg/s respectively. It was found that a higher water inlet temperature caused higher temperatures of window components due to the greater amounts of radiative and convective heat dissipated by the copper tubing.

4. Multiple windows interconnection

In smart window panes water may enter the different units either in parallel or in series configuration. In the parallel configuration, each unit gets water from the main source with the same initial water temperature with the advantage that the solar cells embedded on the copper tubes will operate at their lowest possible temperature, which in turn maximizes its electrical output depending on the intensity of the incident solar radiation and ambient and water temperatures. A drawback of this configuration is that thermal gain represented by the outlet temperatures would be relatively low requiring higher auxiliary heating energy to meet a specific domestic hot water demand.

In the series configuration several units are sequentially connected with water coming out of one unit being inputted to the next unit and so on. The advantage of such arrangement is a high water outlet temperature with a downside being a higher PV cell temperature. The number of units that could be sequentially connected is subject to the limits imposed by the solar cell temperature achieved in the farthest downstream stages and physical and electrical properties of solar cells.

Fig. 16 shows predicted thermal behaviour of two window units connected sequentially for a system operating with a direct solar radiation intensity of 800 W/m^2 with a constant ambient temperature of 273 K, a water inlet temperature of 283 K and a water flow rate, 0.01 kg/s. Solar cell temperature increased from 283 K (the first cell in the first unit) to 313 K (the last cell in the second unit) i.e. an increase of 30 K for just two units connected in series. It is predicted that a sequential connection for a number of window units, ten units for example, will lead to operating temperatures for solar cells which are too high and accordingly impair solar cells electrical output.

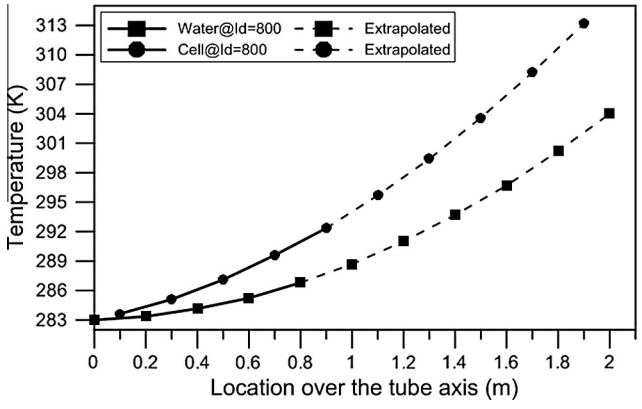

Fig. 16. Solar cells and water temperatures predicted at different locations along the tube axis for the first window unit (solid) and extrapolated to predict the solar cells and water temperatures for the second window unit in case of sequential connection (dotted).

One option for sequential connection is to increase the water flow rate; this will result in reduction in both water outlet temperature and solar cells temperatures as indicated in Fig. 8.

5. Conclusions

A validated CFD model has been developed to predict the thermo-fluid performance of a novel Smart Window configuration accounting for the convective, radiative and conductive heat transfer processes occurring in the window components. Two window segments have been modelled; a horizontal window segment of dimensions 1 m by 0.2 m and a vertical window segment of dimensions 0.2 m by 1 m; both containing five equally spaced concentrator units with concentration ratio of 500×. Temperatures of coolant water and solar cells have been predicted at different locations within the segments simulated. Temperatures have been predicted for different environmental and physical conditions including solar radiation intensity, ambient and water inlet temperature, and water flow rate.

Smart Windows have been shown to be a promising and effective way to control solar radiation transmitted through windows to the building interiors whilst enabling gain of both electrical and thermal energy from the unwanted direct solar radiation rather than simple rejection of such a radiation component obtained using traditional blinding.

Acknowledgements

The authors would like to acknowledge the support of the Engineering and Physical Sciences Research Council (UK) for their support through research grant EP/D060214/2, Development of a Novel Tunnel-junction-free Concentrator Cell and its Evaluation for a Smart Windows Application. The authors would like also to acknowledge Ashkan Davoodi of CD-Adapco for his help.

References

Adams, J.G.J., Browne, B.C., Ballard, I.M., Connolly, J.P., Chan, N.L.A., Ioannides, A., Elder, W., Stavrinou, P.N., Barnham, K.W.J., Ekins-Daukes, N.J., 2011. Recent results for single-junction and tandem quantum well solar cells. Prog. Photovoltaics Res. Appl. 19, 865–877.

Bange, K., 1999. Colouration of tungsten oxide films: a model for optically active coatings. Sol. Energy Mater. Sol. Cells 58, 1–131.

DeForest, N., Shehabi, A., Garcia, G., Greenblatt, J., Masanet, E., Lee, E.S., Selkowitz, S., Milliron, D.J., 2013. Regional performance targets for transparent near-infrared switching electrochromic window glazings. Build. Environ. 61, 160–168.

Kern, E.C., Russell, M.C., 1978. Combined photovoltaic and thermal hybrid collector systems. In: Presented at the Institute of Electrical and Electronics Engineers Photovoltaic Specialists Conference, Washington DC, USA. pp. 1153–1157.

Kim, J.-H., Park, Y.-J., Yeo, M.-S., Kim, K.-W., 2009. An experimental study on the environmental performance of the automated blind in summer. Build. Environ. 44, 1517–1527.

Piccolo, A., Simone, F., 2009. Effect of switchable glazing on discomfort glare from windows. Build. Environ. 44, 1171–1180.

Rohr, C., Abbott, P., Ballard, I., Connolly, J.P., Barnham, K.W.J., Mazzer, M., Button, C., Nasi, L., Hill, G., Roberts, J.S., Clarke, G., Ginige, R., 2006. InP-based lattice-matched InGaAsP and strain-compensated InGaAs/InGaAs quantum well cells for thermophotovoltaic applications. J. Appl. Phys. 100, 114510.

Safer, N., Woloszyn, M., Roux, J.J., 2005a. Three-dimensional simulation with a CFD tool of the airflow phenomena in single floor double-skin facade equipped with a venetian blind. Sol. Energy 79, 193–203.

Safer, N., Woloszyn, M., Roux, J.-J., Rusaouën, G., Kuznik, F., 2005b. Modeling of the double-skin facades for building energy simulations: radiative and convective heat transfer. In: Building Simulation 2005. Presented at the Ninth International IBPSA Conference, Montréal, Canada, pp. 1067–1074.

Shih, T.-H., Liou, W.W., Shabbir, A., Yang, Z., Zhu, J., 1994. A new k-eddy viscosity model for high Reynolds number turbulent flows model development and validation, NASA TM 106721.

Tripanagnostopoulos, Y., Siabekou, C., Tonui, J.K., 2007. The Fresnel lens concept for solar control of buildings. Sol. Energy 81, 661–675.

Vats, K., Tiwari, G.N., 2012. Energy and exergy analysis of a building integrated semitransparent photovoltaic thermal (BISPVT) system. Appl. Energy 96, 409–416.